SCIENTIA PLENA
www.scientiaplena.org.br
VOL. 18, NUM. 9 2022
doi: 10.14808/sci.plena.2022.094201

Carvão ativado de baixo custo da casca da castanha do Pará para remoção de corante em solução aquosa: estudo cinético e do mecanismo termodinâmico

Low-cost activated carbon from the husk of Pará nuts for dye removal from aqueous solution: kinetic and thermodynamic mechanism study

L. O. Santos[1], D. L. Oliveira[1]; E. D. Nascimento[2]; W. S. de Alencar[1]; J. L. P. Siqueira[1]; D. A. Vieira[1,3]; A. D. V. de Souza[1], F. A. O. Carvalho[1,*]

[1]*Federal University of São Carlos Sul and Sudeste of Pará, 68505-080, Marabá- PA, Brazil*
[2]*Department of Chemistry, Federal University of São Carlos-UFSCar, 13565-905, São Carlos-SP, Brazil*
[3]*Federal University of Paraíba, João Pessoa-PB, Brasil*

**adriano.carvalho@unifesspa.edu.br*
(Recebido em 05 de abril de 2022; aceito em 13 de agosto de 2022)

Foi utilizado o carvão ativado produzido a partir da casca da castanha do Pará, *Bertholletia excelsa*, como alternativa ecológica e de baixo custo para a adsorção do corante laranja 16 reativo (RO-16). O material adsorvente CA-700^{325} foi sintetizado por meio da carbonização da biomassa da castanha do Brasil a 700 ºC por 2h para a obtenção de carvão ativado com alta capacidade adsortiva. A caracterização superficial foi realizada por FTIR e BET. As isotermas de Langmuir, Freundlich e Temkin foram utilizadas para descrever o equilíbrio de adsorção, enquanto a cinética de adsorção foi estudada usando modelos de pseudo-primeira ordem, pseudo-segunda ordem, Elovich e difusão intrapartícula. A remoção do RO-16 depende do pH do meio, atingindo um índice máximo em pH 1,0. Na dosagem de 5,0 g/L, a remoção de RO-16 foi maior que 99%. As isotermas de adsorção tiveram um melhor ajuste dos dados experimentais com o modelo de Langmuir, revelando que a adsorção de RO-16 no CA-700^{325} ocorre em monocamada, com capacidade máxima de adsorção em monocamada de 154,8 mg/g, equilíbrio de adsorção aparece em 150 min e a cinética de adsorção segue o modelo de pseudo-segunda ordem. O presente estudo relata que o material de baixo custo é muito promissor para o tratamento de efluentes da indústria têxtil.
Palavras-chave: adsorção, carvão ativado, laranja reativo 16.

The use of activated carbon produced from the husk of Pará nuts, *Bertholletia excelsa*, as an ecological and low-cost alternative for the adsorption of reactive orange 16 dye (RO-16) was used. The adsorbent material, CA-700^{325}, was synthesized by carbonizing the biomass of Brazil nuts at 700 ºC for 2h in order to obtain activated carbon with high adsorptive capacity. The superficial characterization was performed by FTIR and BET. Langmuir, Freundlich and Temkin isotherms were used to describe the adsorption equilibrium, while the adsorption kinetics was studied using pseudo-first order, pseudo-second order, Elovich and intraparticle diffusion models. The removal of RO-16 depends on the pH of the medium, reaching a maximum index at pH 1.0. At a dosage of 5.0 g/L, the removal of RO-16 was greater than 99%. Adsorption isotherms had a better fit of the experimental data with Langmuir model, revealing that the adsorption of RO-16 in the CA-700^{325} occurs in a monolayer, with a maximum capacity of adsorption in a monolayer of 154.8 mg/g, the adsorption equilibrium appears in 150 min and that the adsorption kinetics follows the pseudo-second order model. The present study reports that the low-cost material is very promising for the treatment of the textile industry effluents.
Keywords: adsorption, activated carbon, reactive orange 16.

1. INTRODUCTION

Water pollution is a major environmental threat that needs immediate attention. Industrial waste contributes considerably to contamination and pollution of surface and groundwater [1]. Effluents from the textile, leather, cosmetic, plastic, pharmaceutical and food processing industries carry large volumes of water contaminated by synthetic dyes, which are difficult to biodegrade, making them unsuitable for further use [1-3]. The textile sector is one of the main responsible for the release of wastewater contaminated by dyes. Currently, about 7×10^7 tons of

synthetic dyes are produced per year in this sector around the world, and about 10% is wasted as effluent [2, 4]. The release of dyes in textile effluents directly impacts salinity, pH and water temperature. In addition, the accumulation of these substances causes a decrease in biological oxygen demand (BOD) as well as an increase in chemical oxygen demand (COD) and suspended solids, also leading to decreased levels of photosynthesis [2, 3, 5-7]. Among the dyes used in this sector, the class of azo dyes constitutes the largest portion, corresponding to 70-80% [2, 8]. Azo dyes have one or more azo groups (-N=N-) in their chemical structure. A significant part of commercially used synthetic dyes is composed of toxic, carcinogenic and mutagenic azo dyes. [1, 9]. Substances such as Benzidine, 3,3-dimethylbenzidine and phenylenediamine (p-PDA), released by the biotransformation process of azo dyes, are reported to cause tumors, allergies and other diseases in humans and in animals [9-11]. Reactive orange 16 (RO-16), whose chemical structure is shown in Figure 1, is an example of an azo dye, which is soluble in water and widely used in order to impart color to natural and synthetic textile fibers, due to its high ability to form covalent bonds with these substrates [12]. However, this dye causes pollution to the environment as a result of its toxicity, and when inhaled or ingested it can lead to adverse effects in the human body, such as respiratory problems, tumors and irritation to the eyes and skin [12]. Therefore, the removal of RO-16 from wastewater becomes an important action to mitigate possible environmental impacts and maintain the integrity of human health.

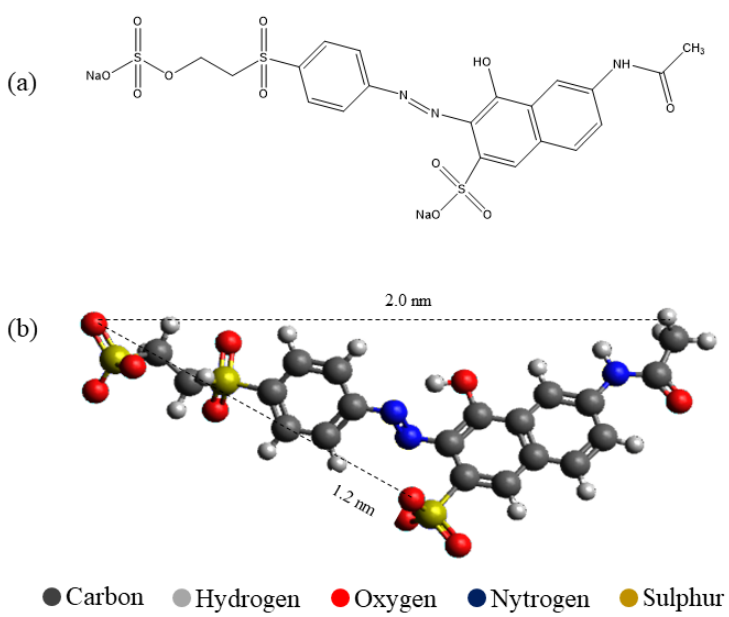

Figure 1: Chemical structure of reactive orange 16 (a) and optimized three-dimensional structural formula of the ionic form of RO-16 using Avogadro 1.2.0 software (b).

Several conventional physical-chemical treatment methods have been successfully used for decolorizing wastewater, such as coagulation [13], photodegradation [14], electrochemical advanced oxidation/electrocoagulation [15], ozonation [16], membrane filtration [17] and adsorption [18]. However, most have disadvantages, such as low efficiency, high cost, generation of high-risk by-products and process delays [1]. Among these methods, adsorption has been regularly used due to its high efficiency, low cost and easy operation. [1, 19]. Adsorption is a dissolution process based on the transfer of atoms, molecules and ions in a solution to a solid material surface called adsorbent [9]. In the adsorption process, a dynamic equilibrium is formed between the concentrations of substances in the solid-liquid phase. This equilibrium is important to measure the adsorptive capacity of the adsorbent material [9]. The surface area, the dissolved substance's type and properties such as the pH of the medium, temperature and type of adsorbent are all factors that can affect the adsorption process. [9, 20].

Activated carbon is a very promising adsorbent for treating dye-contaminated effluents, considering its high adsorptive capacity, high surface area and fast adsorption kinetics [21, 22].

However, the access to commercial activated carbon remains limited due to its high cost, which results from the use of non-renewable sources and the expensive materials used during synthesis [23]. Thus, many studies are being centered on the production of activated carbon from low-cost and ecological precursors that have a high adsorptive capacity, such as those from plant extraction. The use of these materials can save financial resources and also reduce the amount of waste in the environment [1, 21]. Given the above, this study addresses the removal of reactive orange 16 (RO-16) from synthetic solution, using activated carbon produced from Pará nut husk as a low-cost bioadsorbent. The material was characterized by BET, BJH and FTIR. It was also analyzed the effect of operational parameters on the adsorption of RO-16, such as adsorbent dosage, pH, contact time and the effect of initial concentrations. The adsorption isotherm was evaluated using the mathematical models of Langmuir, Freundlich and Temkin, while the adsorption kinetics was assessed using pseudo-first order, pseudo-second order, Elovich and intraparticle diffusion models.

2. 2. MATERIALS AND METHODS

2.1 Activated carbon preparation and characterization

The residue (Pará nut husk) was collected in large quantities at a farmers market located in the city of Marabá-PA, Brazil. After collection, the residue was washed several times in running water, left to rest in water for 24 h and then dried in an oven at 80 ºC for 48 h. In the next step, it was crushed in a knife mill (NL-226/02) and sieved to obtain powdered particulate material with a size of 0.045 mm (325 mesh). This procedure was performed several times until a substantial amount of material was gathered. The powdered material was carbonized in a muffle furnace at 700 ºC for 2h to obtain activated carbon with high adsorptive capacity [24]. The activated carbon, named CA-700^{325}, was stored in a sealed plastic bottle for future experiments.

The textural properties of CA-700^{325} were determined by adsorption-desorption of N_2 at 77.35 K using a surface analyzer (QUANTACHROME NOVA 2200e) with liquid nitrogen in a density of 0.808 g cm^{-3}. Before taking the measurements, the sample was subjected to a thermal pretreatment at 423 K for 2 h. The adsorption-desorption of N_2 in the sample was used to calculate the specific surface area (S_{BET}) through the BET method (Brunauer – Emmett – Teller). The diameter (D_p) and the pore-size distribution were determined by the BJH method (Barrett – Joyner – Halenda). The functional groups existing in the material were evaluated by Fourier Transform Infrared Spectroscopy Analysis (FTIR) in ATR mode, using a Thermo spectrometer (Nicolet iS50 FT-IR), in the scanning range of 4000-400 cm^{-1}, 100 scans and resolution 4 cm^{-1}. Data acquisition was performed using the software OMNIC and the data was analyzed using the software origin, version 8.0. As a pre-treatment, the samples were dried at 105 °C for 24 hours.

2.2 Stock solution preparation

The Reactive Orange 16 dye (RO-16), ID 329751987, 617 molecular mass, $C_{20}H_{17}N_3Na_2O_{11}S_3$, with 70% content was purchased from the company Sigma-Aldrich, Saint Louis, USA. The 1000 mg L^{-1} stock solution was prepared by dissolving a mass amount of RO-16 in 1000 mL of ultrapure water in the volumetric flask. Subsequently, the bottle was completely covered with aluminum foil to minimize contact with light and external influences. The stock solution was properly stored until the adsorption tests were carried out.

2.3 Analytical curve

From the stock solution, other solutions were prepared by diluting aliquots into 2 mL microtubes in the concentration range of 2.5 to 27.5 mg L^{-1}, in order to quantify the residual concentration of RO-16 in the adsorption tests. Readings were taken on a spectrophotometer (Bel Spectro S05), at the maximum absorption wavelength of 493 nm. The experiments for the

analytical curve obtention were carried out in triplicate, in a quartz cuvette with an optical path of 1 cm and 1 mL.

2.4 Description of experimental procedures

Adsorption experiments were conducted using 100 mL of RO-16 solution added to 125 mL Erlenmeyer flasks. Adsorbent masses were added to RO-16 solutions and the mixtures were shaken in an orbital shaker incubator (SL-223), at 200 rpm, 20 ºC and contact time of 180 min. The initial pH of the solutions was adjusted with HCl or NaOH (0.2 mol L^{-1}). The experiments were used to evaluate the influence of RO-16 adsorption on parameters such as adsorbent dosage (1-10 g L^{-1}), solution pH (1-9), contact time (1-300 min) and initial concentrations of RO-16 dye (50-200 mg L^{-1}). The adsorption isotherms studies were carried out for dye concentrations varying between 50 to 300 mg L^{-1} at 20 ºC. At the end of the experiments, the supernatant solutions were removed, filtered at 3000 rpm for 8 min and read in a spectrophotometer (Bel SpectroS05) at 493 nm [9]. The removal percentage was calculated by Equation 1.

$$Removal\ (\%) = \frac{C_0 - C_e}{C_e} x100 \quad (1)$$

where C_0 (mg L L^{-1}) and C_e (mg L L^{-1}) are the initial and equilibrium concentrations of the dye in solution, respectively.

3. 3. RESULTS AND DISCUSSION

3.1 Adsorbent characterization

3.1.1 Surface area and porosity assessment

The adsorption-desorption isotherm of N_2 at 77 K for CA-700[325] and the pore size distribution are shown in Figures 2a and b respectively.

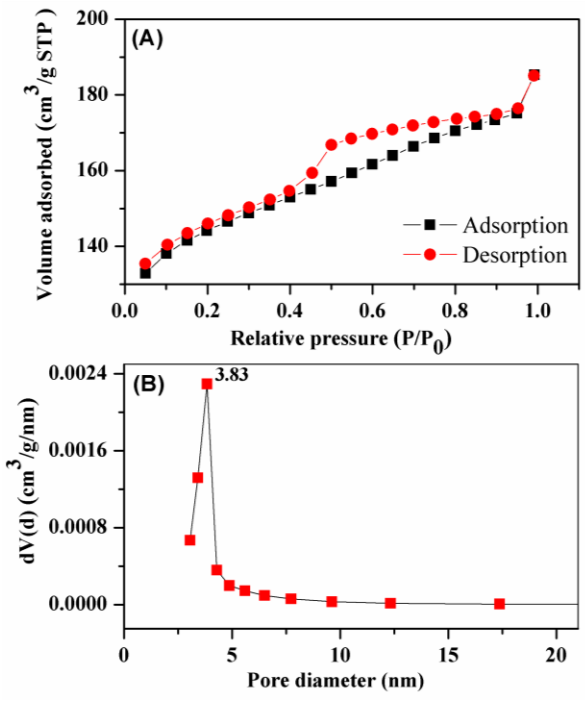

Figure 2: Nitrogen adsorption–desorption isotherm (a) and pore size distributions (b) of CA-700[325].

The adsorption-desorption isotherm profile of N_2 for CA-700^{325} (Figure 2A) fits in type IV, based on the classification established by the International Union of Pure and Applied Chemistry (IUPAC) [25], with H_3-type hysteresis loop corresponding to partial pressure $P/P_0 =$ 0.4 to 0.99 , which suggests the predominant occurrence of mesopores in the material [1]. The specific surface area (S_{BET}) determined by the BET method was 461.385 m^2 g^{-1}, while the surface area and pore volume obtained by the BJH method were 61.631 m^2 g^{-1} and 0.079 cm^3 g^{-1}, respectively. According to Figure 2 (B), the CA-700^{325} pore size distribution ranged between 3 and 20 nm. However, the largest pore volume was provided by those with a diameter of 3.83 nm, indicating that the adsorbent is mesoporous, since the diameter of mesoporous materials ranges between 2.0 and 50 nm [1]. The greatest distance between the atoms located at the extremes of the reactive orange 16 molecule is 2.0 nm (Fig. 1b), while the CA-700^{325} mesopores diameter is 3.83 nm, the ratio of these measurements being equal to 1.91. Thus, CA-700^{325} can accommodate a dye molecule that diffuses from the volume of solution to the pores of the adsorbent [26].

3.1.2 CA-700^{325} FTIR analysis

Figure 3 shows the result of Fourier Transform Infrared Spectroscopy (FTIR) analysis for both Brazil nut husk biomass and CA-700^{325}, considering the range of 4000 to 400 cm^{-1}.

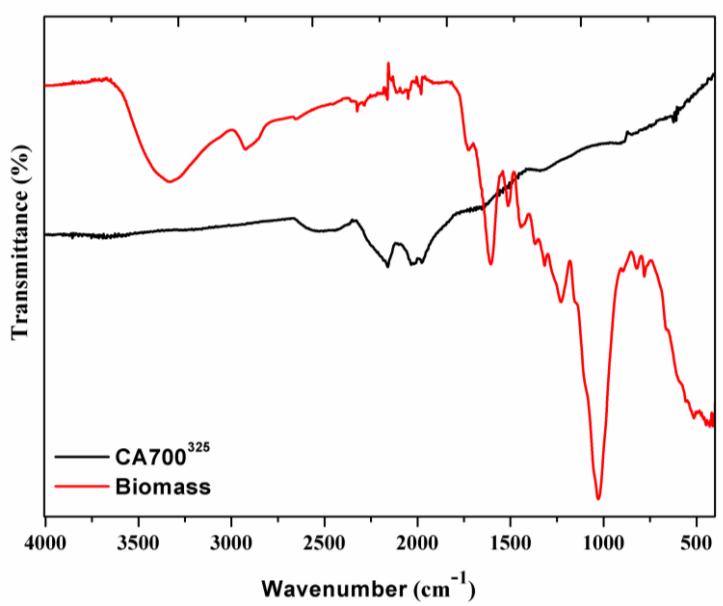

Figure 3: The FTIR spectrum of biomass and CA-700^{325}.

The carbon matrix not only consists of carbon atoms, but is also formed by heteroatoms, including oxygen, nitrogen, halogen, sulfur, phosphorus, and others. The surface chemistry of activated carbon is governed by these species bonded to carbon atoms [25]. The FTIR spectrum of Brazil nut husk biomass is characterized by the presence of a wide and accentuated band at 3330 cm^{-1} corresponding to the O-H stretching vibrations of alcohols, phenols and carboxylic acids present in pectin, lignin and cellulose, thus showing the presence of free hydroxyl groups on the biomass surface [27, 28]. The peak centered at 2926 cm^{-1} indicates the presence of the -C-H stretching in -CH_2, -CH_3 or - (CH_2)n in cellulose, hemicellulose and lignin [27, 29]. The band located at 1735 cm^{-1} corresponds to the presence of the carbonyl group (C=O), natural in hemicellulose and lignin, and the band at 1613 cm^{-1} corresponds to the C=C stretching vibrations of aromatic compounds [27, 30-32]. The band at 1518 cm^{-1} could be assigned to amine groups with N-H [33] and at 1035 cm^{-1} to C-O-C [27, 31]. It is visible that the biomass

carbonization promoted drastic changes in the functional groups, which is evidenced by an intense reduction in the contributions of oxygenated groups. In the CA-700^{325} spectrum, low intensity remnant bands were observed at 2159, 2033, 1977 cm^{-1}, indicating the material partial degradation by pyrolysis [27, 31].

3.2 Effect of operating parameters on RO-16 adsorption

3.2.1 Effect of adsorbent dosage and solution pH

The study of adsorbent dosage in the percentage of RO-16 removal was carried out in the range of 1.0 to 10.0 g L^{-1}, pH 6, at 20 ºC, contact time of 180 min and dye concentration of 100 mg L^{-1}. Figure 4a shows the experimental result for adsorbate adsorption.

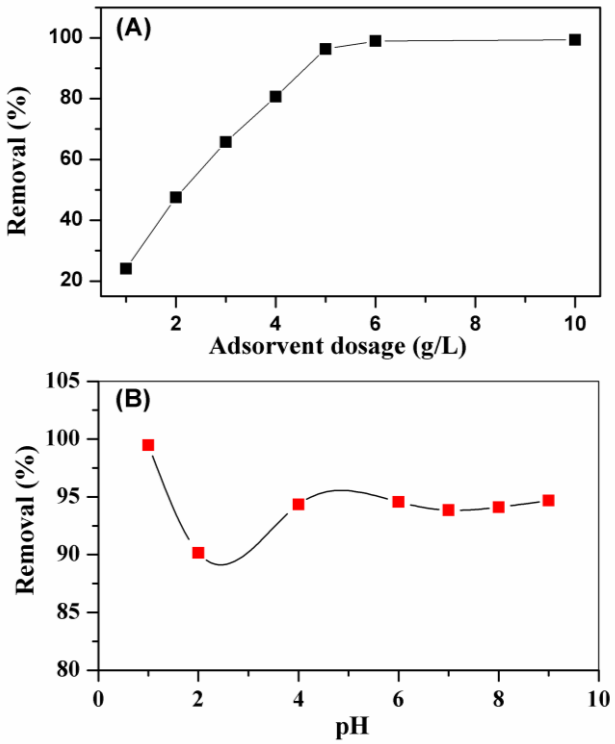

Figure 4: Study of mass dosage in the adsorption of dye RO-16 onto CA-700^{325} (a), and study of the effect of pH on the adsorption of RO-16 onto CA-700^{325} at a concentration of 100 mg L^{-1}, dosage of 5g L^{-1} and contact time of 180 min (b).

According to Figure 4A, the CA-700^{235} dosage increase promoted an expressive increase in the dye removal. The percentage of removal increased from 24.1 to 96.34% when the doses were 1 and 5 g L^{-1}, respectively. For higher adsorbent concentrations (6 and 10 g L^{-1}), a saturation of the material is observed, with the removal remaining constant at 99.3%. The increased removal is attributed to the greater availability of sites for the adsorbate [34, 35]. On the other hand, the increase in the adsorbent mass promoted a decrease in the adsorptive capacity per gram, a behavior observed in several studies with RO-16 [19, 26, 34]. In another study, a lower removal (90%) of RO-16 by activated carbon from coconut husk was reported at a dosage of 5 g L^{-1}, time of 25 h and initial concentration of 100 mg L^{-1} [18]. A removal of 97.25% at the dosage 10 g L^{-1} and initial concentration of 100 g L^{-1} was achieved in the adsorption of RO-16 using modified kenaf core fiber, a similar result to that reported in this study [19]. A maximum removal of 96% was observed at a dosage of 2.5 g L^{-1}, initial concentration of 300 mg L^{-1} and time of 4h for the adsorption of RO-16 by activated carbon obtained from the pine fruit husk [34]. Despite the better removal rates achieved by the dosages

of 6 and 10 g L^{-1}, it was decided to use 5 g L^{-1} as the standard dose of CA-700^{325} to carry out further studies, aiming at the economy of the adsorbent. In the adsorption process, pH plays an important role, influencing the degree of ionization of the adsorbed molecule and the adsorbent surface charges, which affects the adsorption capacity [36]. Thus, the removal capacity study of RO-16 in CA-700^{325} was carried out in order to evaluate the effect of pH. Figure 4B shows the dye adsorption behavior at pH 1.0, 2.0, 4.0, 6.0,7.0, 8.0 and 9.0. According to Figure 4B, the removal percentage is maximum at pH 1, being 99.5%. Although a marked reduction in pH 2 is observed, removal rates are greater than 90% throughout the range. Previous studies show that the removal of RO-16 dye in activated carbon is favored at acidic pH, with rates higher than 80% [18, 26, 34]. The high removal of CA-700^{325} over a wide pH range indicates that this material has a high potential for the analyte remediation in industrial effluents. In this study, the RO-16 adsorption mechanism was proposed as follows [9].

Initially, the dye is dissolved in an aqueous solution and the sulfonate groups (R – SO_3Na) dissociate and form into ions (R-SO_3^-) and Na^+, according to reaction 1.

1) $R\text{-}SO_3Na + H_2O \rightarrow R\text{–}SO_3^- + Na$

In a second step, the adsorption process occurs by electrostatic interactions and Van der Waals forces between the surface of CA-700^{325} and the RO-16 SO_3^- ions, according to reaction 2.

2) $(R – SO_3^- + Na^+)$ + CA700^{325} surface → Adsorption of RO-16

Adsorption increased with decrease pH of dye solution, probably due to protonation of the absorbent surface [18]. However, adsorption decreased as a result of competition between OH^- and SO_3^- ions for the absorbent surface with increasing solution alkalinity [1, 9].

3.2.2 Effect of contact time and initial concentrations

Figure 5 shows the effect of contact time (1 - 300 min) and initial concentrations (50, 75, 100, 150 and 200 mg L^{-1}) on the adsorption of RO-16 using a dosage of 5 g L^{-1}, at 20 ºC and pH 6.

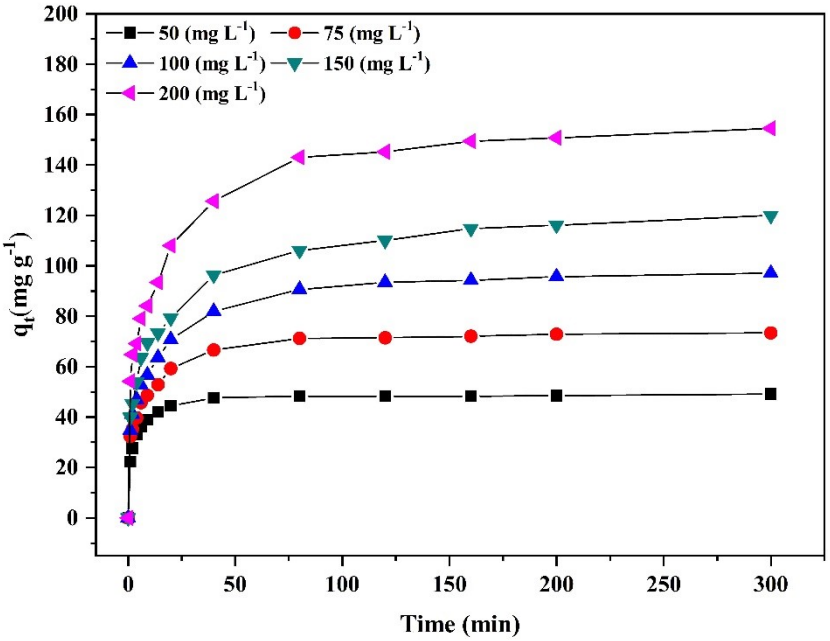

Figure 5: Effects of contact time and initial concentration on the adsorption of RO-16 onto CA-700^{325} at 20 °C.

The kinetic curve shows that RO-16 removal is considerably fast in the first 20 min, then it continues at a slower rate (20-120 min) and reaches equilibrium around 150 min, when the material saturation occurs. An equilibrium time of 23 h was reported for the RO-16 adsorption on fish scale activated carbon [26] and 2 hours for activated carbon obtained from *Ananas comosus* [37], showing that equilibrium time depends on the absorbent nature. The fast removal and the fact that equilibrium was reached in 150 min indicate that CA-700^{325} is efficient. The high rate of dye adsorption in the initial minutes is associated with greater availability of adsorbent sites [38, 39], however, as they are occupied, the inverse process (desorption) speed is favored and the adsorption rate decreases [19]. This reduction is likely caused by repulsive forces between the adsorbate molecules as sites are occupied, and by saturation of sites available for adsorption [26, 36, 38]. The maximum adsorption capacity escalates from 47.4 to 143.5 mg g^{-1} with the increase in the RO-16 initial concentration from 50 to 200 mg L^{-1}, leading to an intensification in the driving force associated with mass transfer and resulting in greater adsorption [40]. Such behavior is also observed in the RO-16 removal by other adsorbents [19, 26, 37].

3.3 Adsorption Kinetics

Kinetic modeling of the adsorption process is important to assess the rate at which the dye is removed from the solution [3]. The kinetic process depends on factors such as solution pH, concentration, nature of the adsorbate, molecular weight, solubility and others. In order to understand the kinetic mechanism controlling the adsorption of RO-16 on CA-700^{325}, experimental data were evaluated using pseudo-first order, pseudo-second order, Elovich and intraparticle diffusion models [3, 41, 42]. The linear expression of the pseudo-first order model, proposed by Lagergren [43] is expressed by Equation 2.

$$ln\,(q_e - q_t) = lnq_e - k_1 t \tag{2}$$

where q_t (mg g^{-1}) and k_1 (min^{-1}) are the equilibrium adsorbed quantity and the pseudo-first order constant [44]. The first-order rate constant k_1 was estimated from the slope of the line (-k) and q_e by intercept (ln q_e) of ln(q_e-q_t) and t. The values of these parameters are presented in Table 1 and the linear fitting in Figure 6 (A). Meanwhile, the result of the pseudo-second order model proposed by Ho and McKay (1998) [45], expressed by Equation 3, is shown in Figure 6.

$$\frac{t}{q_t} = \frac{1}{q_e^2 k_2} + \frac{1}{q_e} t \tag{3}$$

where k_2 (g $mg^{-1}min^{-1}$) and q_e (mg g^{-1}) are the second-order rate constant and the equilibrium adsorbed amount, respectively. [42]. Similarly, the constant k_2 is measured through the intercept ($1/q_e^2\,k_2$) of t/q_t and t. Zeldowitsch's equation (Equation 4) [46], which is currently known as the Elovich model, was initially developed for the kinetic study of chemical gas adsorption [47]. The linear fitting for this model is shown in Figure 6 (C).

$$q_t = \frac{1}{b}\ln(ab) + \frac{1}{b}\ln(t) \tag{4}$$

where a (mg $g^{-1}min^{-1}$) and b (mg g^{-1}) are the initial adsorption rate and the desorption constant, respectively. The value of b was obtained by the slope of the line 1/b and the value of a by the intercept of the line (1/b ln(ab)) of q_t versus (ln (t)). The values of these parameters are shown in Table 1. Finally, the result of applying the intraparticle diffusion kinetic model proposed by Weber and Morris [48], as per Equation 5, is shown in Figure 6 (D).

$$q_t = k_{dif} t^{1/2} + C \quad (5)$$

where k_{dif} (mg g^{-1}min$^{1/2}$) and C are the intraparticle diffusion constant and the boundary layer thickness, respectively.

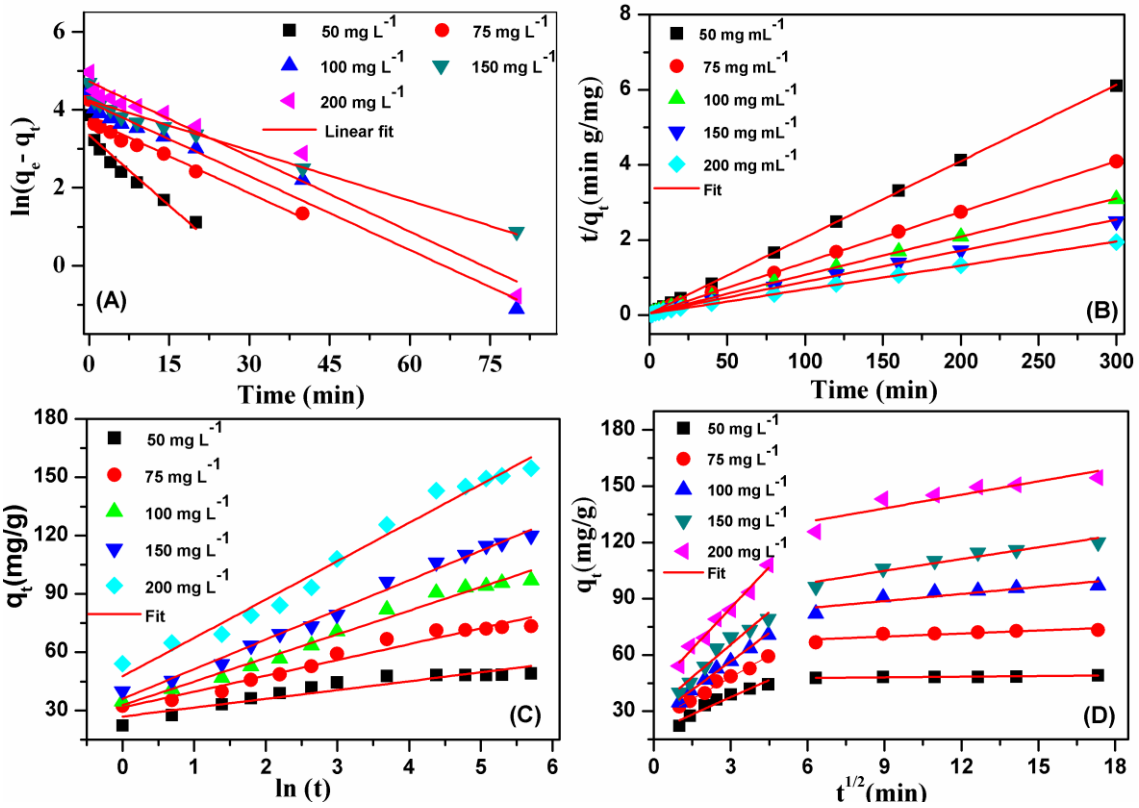

Figure 6: Fits of the experimental data to the linearized equations of the kinetic models (a) Pseudo-first order, (b) Pseudo-secund order, (c) Elovich and (d) intraparticle diffusion.

The values of the correlation coefficients R^2_{adj}, shown in Table 1, and the linear fitting (Figure 6) show that the pseudo-second order kinetic model (Figure 6B), whose fits presented values of $R^2_{adj} > 0.99$ for all initial concentrations, describes the RO-16 adsorption mechanism. Better correlations to this model for the adsorption of RO-16 are portrayed in studies with low-cost activated carbon from precursors such as *Ananas comosus* [37], rice husk [3], fish scale [26], coconut husk [18] and sawdust [49]. The best fit of experimental data to the pseudo-second order kinetic model shows that the adsorption rate of RO-16 in CA-700^{325} does not depend on the concentration of dye in the solution, but on the availability of adsorbent sites [26]. In addition, it was observed that the values of the pseudo-second order model constant, k_2, decreased from 9.9 x10^{-3} to 9.0 x10^{-4} g/mg/min with the increase of the initial concentration from 50 to 200 mg L^{-1}, respectively. This behavior may be related to competition for the adsorbent sites. At lower concentrations, competition for sites is not very intense, which makes the adsorption rate high (higher values of k_2). However, when the concentration increases, the competition for the sites also increases, leading to a lower adsorption rate [26, 50]. Another parameter that contributes to determining the predominant kinetic mechanism in the adsorption process is the proximity between the values of q_e calculated by theoretical ($q_{e,cal}$) and experimental ($q_{e,exp}$) models, in this case, the closer the proximity between these parameters, the greater the applicability of the model [18, 37]. Table 1 shows that the values of $q_{e,cal}$ by the pseudo-second order model are closer to the values of $q_{e,exp}$ when compared to the pseudo-first order model. This result confirms the agreement of the pseudo-second order model with the experimental data.

Table 1: Calculated kinetic parameters for the adsorption of RO-16 onto CA-700[325] at various concentrations.

	Initial concentration (mg L^{-1})				
	50	75	100	150	200
$q_{e,\ exp}$ (mg g^{-1})	47.4	70.5	91	108.5	143.5
Pseudo-first order kinetic					
$q_{e,\ cal}$ (mg/g)	28.5	43.1	66.3	69.3	112.9
k_1 (min^{-1})	0.120	0.063	0.063	0.043	0.064
R^2_{adj}	0.9101	0.9346	0.9732	0.9701	0.9586
Pseudo-secund order kinetic					
$q_{e,\ cal}$ (mg g^{-1})	49.3	74.1	98.3	120.9	156.5
k_2 (g/mg/min)	0.0099	0.0035	0.0017	0.0011	0.0009
R^2_{adj}	0.9999	0.9998	0.9995	0.9986	0.9992
Elovich model					
a (mg/g/ min)	1698.8	391.8	179.7	161.7	219.5
b (g/mg)	0.2200	0.1227	0.0822	0.0655	0.0506
R^2_{adj}	0.8872	0.9639	0.9825	0.9908	0.9772
Intra particle diffusion					
$*K_{dif\ 1}$ (mg/g/$min^{1/2}$)	4.58	6.64	8.84	10.43	13.36
$*K_{dif\ 2}$ (mg/g/$min^{1/2}$)	0.116	0.276	0.742	1.664	1.408
$*C_1$ (mg/g)	22.560	27.299	29.108	33.302	44.037
$*C_2$ (mg/g)	46.967	68.640	84.711	92.091	130.56
$R^2_{adj\ (dif,1)}$	0.8579	0.9708	0.9785	0.9631	0.9855
$R^2_{adj\ (dif,2)}$	0.7646	0.9389	0.9267	0.9512	0.9681

*k_{dif} (mg g^{-1} $min^{½}$) and C are intraparticle diffusion constant and the boundary layer thickness.

Linear fitting of the Elovich (Figure 6C) and intraparticle diffusion (Figure 6D) models showed a correlation coefficient R^2_{adj} ranging from 0.8872 to 0.9771 and 0.7646 to 0.9855, respectively. The values of R^2_{adj}, lower than those obtained by the pseudo-second order model, reveal that these models are not adequate to describe the adsorption kinetics of RO-16 in CA-700[325]. Intraparticle diffusion is the only controlling step of the process if the graph of q_t versus $t^{1/2}$ passes through the origin, that is, C equals 0. If this does not occur, the mechanism is accompanied by other steps [18, 39, 51]. From Figure 6(D) it can be observed that the RO-16 adsorption process occurs in two consecutive steps: the first corresponds to the rapid adsorption on the external surface, that is, the dye molecules are transferred to the easily accessible active sites of the adsorbent and the second denotes the intraparticle diffusion where the adsorption stage is gradual and slow [18, 37, 52, 53].

3.4 Adsorption isotherm

Langmuir, Freundlich and Temkin isotherms were used in order to evaluate the adsorption equilibrium data between RO-16 and CA-700[325]. The parameters obtained through these isotherms provided important information about the adsorption mechanism and surface properties of the adsorbent [3, 38]. The parameters of the Langmuir isotherms [54] were determined from Equation.6.

$$\frac{C_e}{q_e} = \frac{1}{k_L q_m} + \frac{1}{q_m} C_e \tag{6}$$

where q_e (mg g^{-1}) and q_m (mg g^{-1}) are the equilibrium adsorption capacity and the maximum adsorption capacity, respectively; k_L (L mg^{-1}) is the Langmuir constant related to adsorption capacity and energy and C_e (mg L^{-1}) is the equilibrium concentration [55]. The values of q_m and

k_L were determined from the C_e/q_e versus C_e graph with slope of 1 /q_m. The results are shown in Table 2. The Langmuir isotherm was related to the separation parameter R_L (Equation 7), which indicates the favorability of the adsorption process [56].

$$R_L = \frac{1}{1+k_L C_0} \quad (7)$$

Table 2: Isotherm parameters for RO-16 adsorption using CA-700^{325} as adsorbents.

Isotherm	Parameters	Value
Langmuir	q_m (mg/g)	154.8
	k_L (L/mg)	0.228
	R^2_{adj}	0.9928
Freundlich	k_f (mg/g)(L/mg)$^{1/n}$	61.89
	n	5.0
	1/n	0.2
	R^2_{adj}	0.8170
Temkin	k_T (L/mg)	19.99
	b_T (J/mol)	125.35
	R^2_{adj}	0.9010

Table 3: Relationship between Langmuir R_L separation factor and initial concentrations.

C_0 (mg/L)	*Langmuir separation factor (R_L)*
50	0.080
65	0.063
75	0.055
85	0.049
100	0.042
115	0.036
130	0.032
140	0.030
150	0.028
200	0.021
250	0.017
300	0.014

R_L describes the adsorption trend, that is, adsorption is favorable when $0 < R_L > 1$, irreversible when R_L equals to 0, linear when R_L equals to 1 and unfavorable when $R_L > 1$ [56]. According to Table 3, the calculated value of R_L is between 0.080 and 0.014 for the concentration range of 50-300 mg L^{-1}. The effect of concentration on the R_L value is best observed by the graph of R_L versus C_0 (Figure. 7), which exhibits exponential features, in which $0 < R_L < 1$. Thus, the R_L value was favorable for monolayer adsorption of RO-16 in CA-700^{325} [56, 57].

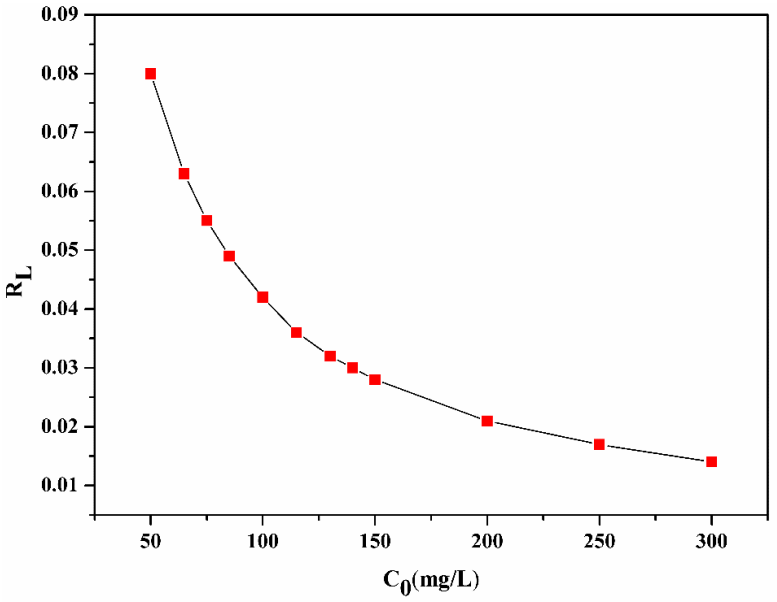

Figure 7: Graphic relationship between Langmuir R_L coefficient and initial RO16 concentrations.

The Freundlich isotherm model applicability [58] to the experimental data was evaluated by Equation 8.

$$lnq_e = lnk_f + \frac{1}{n} lnC_e \quad (8)$$

where n is a dimensionless number associated with adsorption intensity and k_f [(mg g^{-1}) (L mg^{-1})$^{1/n}$] is the Freundlich constant [59, 60]. The values of k_f e n were estimated from the lnq_e versus lnC_e graph with slope of 1/n and intercept ln k_f. The results are shown in Table 2. The favorability of the model is characterized in terms of the magnitude of (n). If n lies between one and ten, this specifies a favorable sorption process. Thus, the value of n = 5 indicates favorability in the adsorption of RO-16 [38]. The linear mathematical model of Temkin isotherm equation [61] is described by Equation 9.

$$q_e = \frac{RT}{b_T} lnk_T + \frac{RT}{b_T} lnC_e \quad (9)$$

where b_T (J mol^{-1}) and k_T (L g^{-1}) are the constant related to the heat of adsorption and the constant of Temkin isotherm, respectively; R (8,314 J mol^{-1} K^{-1}) is the universal gas constant and T (K) is the absolute temperature used in the experiment. The value of b_T was measured from the slope of the line RT/b_T, while the constant k_T was estimated by the intercept RT/b_T lnk_T . The results are shown in Table 2.

Figure 8 shows the linear fitting for the Langmuir, Freundlich and Temkin isotherm models, at 20 ºC and for the initial concentrations of 50, 65, 75, 85, 100, 115, 130, 140, 150, 200, 250 and 300 mg L^{-1}.

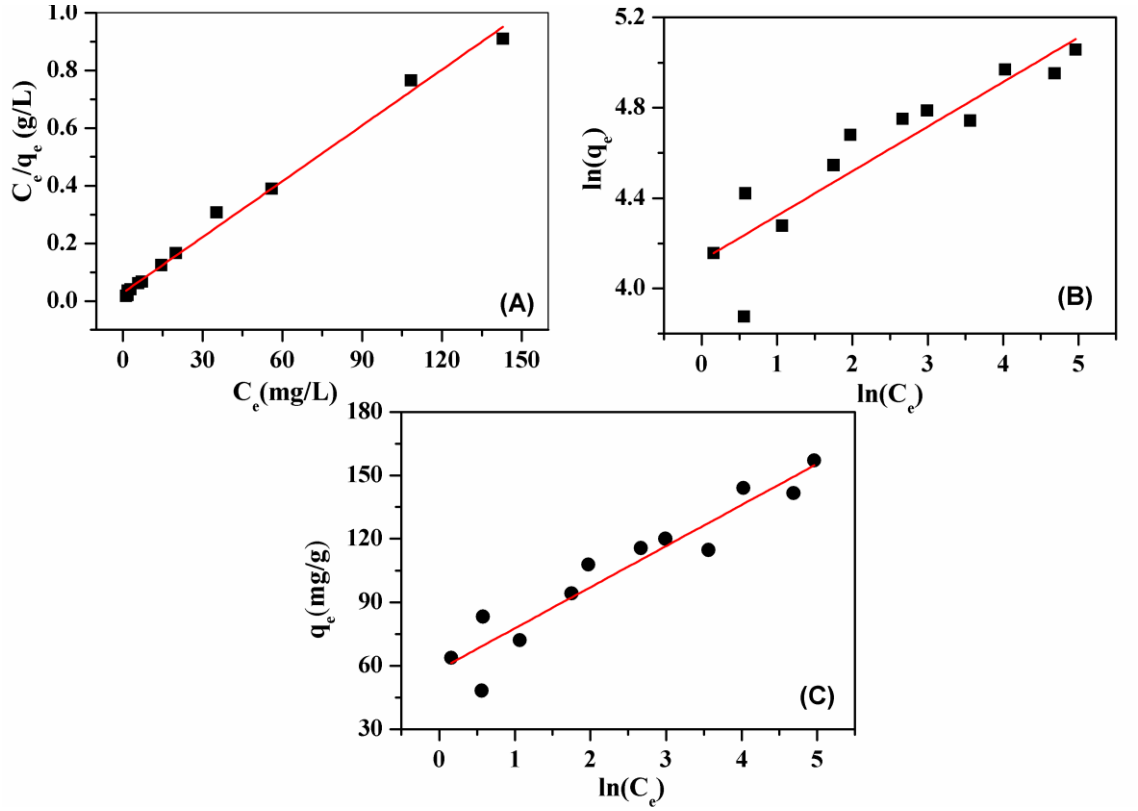

Figure 8: Fits of the experimental data to the linearized equations of the Langmuir, Freundlich and Temkin models.

The linear correlation coefficients (R^2_{adj}), presented in Table 2 and the linear fitting revealed that the RO-16 adsorption process is better explained by the Langmuir model (Figure 8A), being observed values of R^2_{adj} that are closer to the unit (R^2_{adj} equal to 0.992 for Langmuir, R^2_{adj} equal to 0.817 for Freundlich and R^2_{adj} equal to 0.910 for Temkin). Better correlations with the Langmuir model in the adsorption of RO-16 were also reported in the studies by Ramachandran [37], using activated carbon from leaves of *Ananas comosus* (R^2_{adj} equal to 0.98), and by Shah [49], using activated carbon made from sawdust (R^2_{adj} equal to 0.99). Other RO-16 adsorption studies report better correlations to the Langmuir model, especially with the use of chitosan [35, 62, 63]. The fit to this model shows a homogeneous distribution of active sites on the CA-700^{325} surface [64]. The results also showed that the adsorption of RO-16 in CA-700^{325} is a dynamic process that occurs by chemisorption, due to the affinity in terms of surface functional groups and binding energy [27, 65, 66]. Through the Langmuir model, a maximum monolayer adsorption capacity of 154.8 mg g^{-1} was obtained. Table 4 shows several adsorbent materials applied in the adsorption of RO-16, along with monolayer adsorbent capacity (q_m).

The CA-700^{325} maximum monolayer adsorption capacity was proved to be high when compared to other adsorbents reported in the literature for the adsorption of RO-16. The CA-700^{325} monolayer removal was superior to that obtained by activated carbon from rice husk [3] and fish scale [26]. Being also superior to materials such as zeolites and polymeric composites [67, 68].

Table 4: Maximum monolayer adsorption capacity for different adsorbent materials.

Adsorbent	T (K)	pH	Time (h)	Dosage ($g\ L^{-1}$)	q_m ($mg\ g^{-1}$)	Ref.
AC from *Bertholletia excelsa*	293	6	5	5	154.8	This study
AC from *Ananas comosus*	303	-	2	1	112.35	[37]
AC prepared from rice husk ash	303	7	-	5	18.69	[3]
Modified kenaf core fiber	303	6.5	24	1	416. 86	[19]
AC from Brazilian-pine fruit shell	303	6	5	2.5	426	[34]
Residual brewery yeast	298	3	48	1	340	[71]
psyllium seed powder	303	4	5	2	206.6	[36]
AC from fish scales	303	-	24	1	105.80	[26]
AC from waste sawdust	303	6	12	2	65.79	[49]
AC from coconut shell	298	-	24	5	74.56	[18]
Cross-linked chitosan	303	-	30	2	190.96	[35]
Polystyrene resin (Amberlyst A21)	298	2	3.33	1	175.13	[73]
Chitosan-glyoxal/ TiO_2 nanocomposite	313	4	35	0.45	390	[39]
Modified zeolite	298	10	2.5	10	12.6	[67]
Various types of sludge	298	2	24	10	86.8-114	[74]
Chitosan-Fly Ash/Fe_3O_4 composite	303	4	0.91	0.08	66.69	[68]

AC (Activated carbon)

It was found that there were no significant adjustments of the experimental data to the Temkin model. Previous studies report that this model is not suitable for describing dye adsorption equilibrium data [69, 70]. This model is commonly used to predict the gas phase adsorption equilibrium, since the adsorption process is more complex in aqueous systems [70, 71]. Several factors including pH, solubility of the adsorbate in the solvent and temperature influence the liquid phase adsorption process. Temkin's equation was proposed assuming a simpler adsorption phenomenon, disregarding many factors existing in adsorption in aqueous media [72].

4. CONCLUSION

Activated carbon produced from Brazil nut husk (CA-700^{325}) proved to be efficient in removing the reactive orange 16 dye. The absorbent surface area determined by the BET method was 461.385 $m^2\ g^{-1}$, having a pore diameter of 3.83 nm. The FTIR evaluation of the functional groups on the absorbent surface indicated the presence of phenols, carboxylic acids, ketones and aromatic compounds. Subsequent studies revealed that material removal is slightly dependent on the pH of the medium. At a dosage of 10 $g\ L^{-1}$, pH 6, concentration of 100 mg L^{-1}, temperature of 20 ºC and contact time of 180 min, the removal of RO-16 was greater than 99%. The adsorption isotherm studies showed a better fit of the experimental data by the Langmuir model, showing that the adsorption of the reactive orange 16 in CA-700^{325} occurs mostly in monolayer, with maximum adsorption capacity per monolayer of 154.8 $mg\ g^{-1}$. The

kinetic study showed that the RO-16 equilibrium time occurs in 150 min and that the pseudo-second order model characterizes the kinetic mechanism of the adsorption process. The present study demonstrates that the low cost synthesized material is very promising for the treatment of textile industry effluents.

5. ACKNOWLEDGMENT

The authors are grateful to the Ceramic Materials Synthesis Laboratory (LABSMAC, Campina Grande, Brazil) for making available the BET and FTIR facilities used in this work. Thanks are due to the Brazilian agencies CNPq (Process number nº 407891/2018-8), and CAPES for partial financial support. Lucas O. Santos is the recipient of an M.Sc. grant from CAPES (Finance Code 001).

6. BIBLIOGRAPHIC REFERENCES

1. Munagapati VS, Wen HY, Vijaya Y, Wen JC, Wen JH, Tian Z, et al. Removal of anionic (Acid Yellow 17 and Amaranth) dyes using aminated avocado (*Persea americana*) seed powder: adsorption/desorption, kinetics, isotherms, thermodynamics, and recycling studies. Int J Phytoremediation. 2021 Jan;23(9):911-23. doi: 10.1080/15226514.2020.1866491
2. Sarkar S, Banerjee A, Halder U, Biswas R, Bandopadhyay R. Degradation of synthetic azo dyes of textile industry: a sustainable approach using microbial enzymes. Water Conserv Sci Eng. 2017 Sep;2(4):121-31. doi: 10.1007/s41101-017-0031-5
3. Akbar Ali AM, Karthikeyan RK, Sentamil Selvan M, Rai MK, Priyadharshini M, Maheswari N, et al. Removal of reactive orange 16 by adsorption onto activated carbon prepared from rice husk ash: statistical modelling and adsorption kinetics. Sep Sci Technol. 2020 Dec;55(1):26-34. doi: 10.1080/01496395.2018.1559856
4. Benkhaya S, M'rabet S, El Harfi AA. review on classifications, recent synthesis and applications of textile dyes. Inorg Chem Commun. 2020 May;115:107891. doi: 10.1016/j.inoche.2020.107891
5. Roy U, Sengupta S, Das P, Bhowal A, Datta S. Integral approach of sorption coupled with biodegradation for treatment of azo dye using *Pseudomonas* sp.: batch, toxicity, and artificial neural network. 3 Biotech. 2018 Mar;8(4):10-5. doi: 10.1007/s13205-018-1215-1
6. Berradi M, Hsissou R, Khudhair M, Assouag M, Cherkaoui O, El Bachiri A, et al. Textile finishing dyes and their impact on aquatic environs. Heliyon. 2019 Nov;5(11):e02711. doi: 10.1016/j.heliyon.2019.e02711
7. Toprak T, Anis P. Textile industry's environmental effects and approaching cleaner production and sustainability: an overview. J Text Eng Fash Technol. 2017 Aug;2(4):429-42. doi: 10.15406/jteft.2017.02.00066
8. Lang W, Sirisansaneeyakul S, Ngiwsara L, Mendes S, Martins LO, Okuyama M, et al. Characterization of a new oxygen-insensitive azoreductase from brevibacillus laterosporus TISTR1911: Toward dye decolorization using a packed-bed metal affinity reactor. Bioresour Technol. 2013 Dec;150:298-306. doi: 10.1016/j.biortech.2013.09.124
9. Yönten V, Sanyürek NK, Kivanç MR. A thermodynamic and kinetic approach to adsorption of methyl orange from aqueous solution using a low cost activated carbon prepared from *Vitis vinifera* L. Surf Interfaces. 2020 Sep;20:100529. doi: 10.1016/j.surfin.2020.100529
10. Sudha M, Saranya A, Selvakumar G, Sivakumar N. Microbial degradation of azo dyes : A review review article microbial degradation of azo dyes. Int J Curr Microbiol Appl Sci.2018;3(2):670-90.
11. Puvaneswari N, Muthukrishnan J, Gunasekaran P. Toxicity assessment and microbial degradation of azo dyes. Indian J Exp Biol. 2006 Aug;44(8):618-26.
12. Gunasegaran M, Ravi S, Shoparwe NF. Kinetic studies of reactive orange 16 (RO16) dye removal from aqueous solution using PIMs. J Phys Conf Ser. 2020;1529:052003. doi: 10.1088/1742-6596/1529/5/052003
13. Mcyotto F, Wei Q, Macharia DK, Huang M, Shen C, Chow CWK. Effect of dye structure on color removal efficiency by coagulation. Chem Eng J. 2021;405:126674. doi: 10.1016/j.cej.2020.126674
14. Senasu T, Chankhanittha T, Hemavibool K, Nanan S. Visible-light-responsive photocatalyst based on ZnO/CdS nanocomposite for photodegradation of reactive red azo dye and ofloxacin antibiotic. Mater Sci Semicond Process. 2021;123:10558. doi: 10.1016/j.mssp.2020.105558
15. Chanikya P, Nidheesh PV, Syam Babu D, Gopinath A, Suresh Kumar M. Treatment of dyeing wastewater by combined sulfate radical based electrochemical advanced oxidation and

electrocoagulation processes. Sep Purif Technol. 2021;254:117570. doi: 10.1016/j.seppur.2020.117570
16. Yang YC, Zeng SS, Ouyang Y, Sang L, Yang SY, Zhang XQ, et al. An intensified ozonation system in a tank reactor with foam block stirrer: Synthetic textile wastewater treatment and mass transfer modeling. Sep Purif Technol. 2021;257:117909. doi: 10.1016/j.seppur.2020.117909
17. Nawaz H, Umar M, Ullah A, Razzaq H, Zia KM, Liu X. Polyvinylidene fluoride nanocomposite super hydrophilic membrane integrated with Polyaniline-Graphene oxide nano fillers for treatment of textile effluents. J Hazard Mater. 2021;403:123587. doi: 10.1016/j.jhazmat.2020.123587
18. Lee JJ. Study on of process arameters for adsorption of reactive orange 16 Dye by activated carbon. J Korea Acad Coop Soc. 2020;21:667-74. doi: 10.5762/KAIS.2020.21.7.667
19. Obaid MK, Abdullah LC, Idan IJ. Removal of reactive orange 16 Dye from aqueous solution by using modified kenaf core fiber. J Chem. 2016;2016:1-8. doi: 10.1155/2016/4262578
20. Balouch A, Kolachi M, Talpur FN, Khan H, Bhanger MI. Sorption kinetics, isotherm and thermodynamic modeling of defluoridation of ground water using natural adsorbents. Am J Anal Chem. 2013;4:221-8. doi: 10.4236/ajac.2013.45028
21. Djilani C, Zaghdoudi R, Djazi F, Bouchekima B, Lallam A, Modarressi A, et al. Adsorption of dyes on activated carbon prepared from apricot stones and commercial activated carbon. J Taiwan Inst Chem Eng. 2015;53:112-21. doi: 10.1016/j.jtice.2015.02.025
22. Norashiddin FA, Kamaruddin MA, Pakir Mohamed Latiff MF, Mohd Hanif MH. Sustainable activated carbon production via microwave for wastewater treatment: A comparative review. Borneo J Resour Sci Technol. 2020;10:1-9. doi: 10.33736/bjrst.2030.2020
23. Alslaibi TM, Abustan I, Ahmad MA, Foul AA. Cadmium removal from aqueous solution using microwaved olive stone activated carbon. J Environ Chem Eng. 2013;1(3):589-99. doi: 10.1016/j.jece.2013.06.028
24. Cechinel MAP, Ulson De Souza SMAG, Ulson De Souza AA. Study of lead (II) adsorption onto activated carbon originating from cow bone. J Clean Prod. 2014;65:342-9. doi: 10.1016/j.jclepro.2013.08.020
25. Kumar A, Jena HM. Preparation and characterization of high surface area activated carbon from Fox nut (*Euryale ferox*) shell by chemical activation with H_3PO_4. Results Phys. 2016;6:651-8. doi: 10.1016/j.rinp.2016.09.012
26. Marrakchi F, Ahmed MJ, Khanday WA, Asif M, Hameed BH. Mesoporous carbonaceous material from fish scales as low-cost adsorbent for reactive orange 16 adsorption. J Taiwan Inst Chem Eng. 2017;71:47-54. doi: 10.1016/j.jtice.2016.12.026
27. Tran TH, Le AH, Pham TH, Nguyen DT, Chang SW, Chung WJ, et al. Adsorption isotherms and kinetic modeling of methylene blue dye onto a carbonaceous hydrochar adsorbent derived from coffee husk waste. Sci Total Environ. 2020;725:138325. doi: 10.1016/j.scitotenv.2020.138325
28. Pathania D, Sharma S, Singh P. Removal of methylene blue by adsorption onto activated carbon developed from *Ficus carica* bast. Arab J Chem. 2017;10:1445-51. doi: 10.1016/j.arabjc.2013.04.021
29. Foo KY, Hameed BH. Microwave assisted preparation of activated carbon from pomelo skin for the removal of anionic and cationic dyes. Chem Eng J. 2011;173(2):385-90. doi: 10.1016/j.cej.2011.07.073
30. Musule R, Alarcón-Gutiérrez E, Houbron EP, Bárcenas-Pazos GM, Pineda-López MR, Domínguez Z, et al. Chemical composition of lignocellulosic biomass in the wood of *Abies religiosa* across an altitudinal gradient. J Wood Sci. 2016;62(6):537-47. doi: 10.1007/s10086-016-1585-0
31. Md Salim R, Asik J, Sarjadi MS. Chemical functional groups of extractives, cellulose and lignin extracted from native *Leucaena leucocephala* bark. Wood Sci Technol. 2021 Jan;55(2):295-313. doi: 10.1007/s00226-020-01258-2
32. Miyah Y, Lahrichi A, Idrissi M, Khalil A, Zerrouq F. Adsorption of methylene blue dye from aqueous solutions onto walnut shells powder: Equilibrium and kinetic studies. Surf Interfaces. 2018;11:74-81. doi: 10.1016/j.surfin.2018.03.006
33. Cid HA, Flores MI, Pizarro J, Castillo XA, Barros DE, Moreno-Piraján JC, et al. Mechanisms of Cu^{2+} biosorption on *Lessonia nigrescens* dead biomass: Functional groups interactions and morphological characterization. J Environ Chem Eng. 2018;6(2):2696-704. doi: 10.1016/j.jece.2018.03.034
34. Calvete T, Lima EC, Cardoso NF, Vaghetti JCP, Dias SLP, Pavan FA. Application of carbon adsorbents prepared from Brazilian-pine fruit shell for the removal of reactive orange 16 from aqueous solution: Kinetic, equilibrium, and thermodynamic studies. J Environ Manage. 2010;91(8):1695-706. doi: 10.1016/j.jenvman.2010.03.013
35. Marrakchi F, Khanday WA, Asif M, Hameed BH. Cross-linked chitosan/sepiolite composite for the adsorption of methylene blue and reactive orange 16. Int J Biol Macromol. 2016;93:1231-9. doi: 10.1016/j.ijbiomac.2016.09.069

36. Malakootian M, Heidari MR. Reactive orange 16 dye adsorption from aqueous solutions by psyllium seed powder as a low-cost biosorbent: kinetic and equilibrium studies. Appl Water Sci. 2018 Oct;8(7):1-9. doi: 10.1007/s13201-018-0851-2
37. Ramachandran P, Vairamuthu R, Ponnusamy S. Adsorption isotherms, kinetics, thermodynamics and desorption studies of reactive orange16 on activated carbon derived from *Ananas comosus* (L.) carbon. J Eng Appl Sci. 2011;6:15-26.
38. Temesgen F, Gabbiye N, Sahu O. Biosorption of Reactive Red Dye (RRD) on activated surface of banana and orange peels: Economical alternative for textile effluent. Surf. Interfaces. 2018;12:151-9. doi: 10.1016/j.surfin.2018.04.007
39. Abdulhameed AS, Mohammad AT, Jawad AH. Modeling and mechanism of reactive orange 16 dye adsorption by chitosan-glyoxal/TiO_2 nanocomposite: Application of response surface methodology. Desalin Water Treat. 2019;164:346-60. doi: 10.5004/dwt.2019.24384
40. Ebrahimian PA, Saberikhah E, Badrouh M, Emami MS. Alkali treated foumanat tea waste as an efficient adsorbent for methylene blue adsorption from aqueous solution. Water Resour Ind. 2014;6:64-80. doi: 10.1016/j.wri.2014.07.003
41. Srivastava VC, Swamy MM, Mall ID, Prasad B, Mishra IM. Adsorptive removal of phenol by bagasse fly ash and activated carbon: Equilibrium, kinetics and thermodynamics. Colloids Surf A Physicoche Eng Asp. 2006; 272(1-2):89-104. doi: 10.1016/j.colsurfa.2005.07.016
42. Dursun AY, Kalayci ÇS. Equilibrium, kinetic and thermodynamic studies on the adsorption of phenol onto chitin. J Hazard Mater. 2005;123(2-3):151-7. doi: 10.1016/j.jhazmat.2005.03.034
43. Ho YS. Citation review of Lagergren kinetic rate equation on adsorption reactions. Scientometrics 2004;59(1):171-7. doi: 10.1023/B:SCIE.0000013305.99473.cf
44. Arasteh R, Masoumi M, Rashidi AM, Moradi L, Samimi V, Mostafavi ST. Adsorption of 2-nitrophenol by multi-wall carbon nanotubes from aqueous solutions. Appl Surf Sci. 2010;256(14):4447-55. doi: 10.1016/j.apsusc.2010.01.057
45. Ho YS, McKay G. Sorption of dye from aqueous solution by peat. Chem Eng J. 1998;70:115-24. doi: 10.1016/S1385-8947(98)00076-X
46. Qiu H, Lv L, Pan BC, Zhang QJ, Zhang WM, Zhang QX. Critical review in adsorption kinetic models. J Zhejiang Univ Sci. 2009 Apr;10(5):716-24. doi: 10.1631/jzus.A0820524
47. Taylor HA, Thon N. Kinetics of chemisorption. J Am Chem Soc. 1952;74(16):4169-73. doi: 10.1021/ja01136a063
48. Aljeboree AM, Alshirifi AN, Alkaim AF. Kinetics and equilibrium study for the adsorption of textile dyes on coconut shell activated carbon. Arab J Chem. 2017;10:3381-93. doi: 10.1016/j.arabjc.2014.01.020
49. Shah JA, Butt TA, Mirza CR, Shaikh AJ, Khan MS, Arshad M, et al. Phosphoric acid activated carbon from *Melia azedarach* waste sawdust for adsorptive removal of reactive orange 16: Equilibrium modelling and thermodynamic analysis. Molecules. 2020;25(9):2018. doi: 10.3390/molecules25092118
50. Cheng Z, Zhang L, Guo X, Jiang X, Liu R. Removal of Lissamine rhodamine B and acid orange 10 from aqueous solution using activated carbon/surfactant: Process optimization, kinetics and equilibrium. J Taiwan Inst Chem Eng. 2015;47:149-59. doi: 10.1016/j.jtice.2014.09.032
51. Brahmi L, Kaouah F, Boumaza S, Trari M. Response surface methodology for the optimization of acid dye adsorption onto activated carbon prepared from wild date stones. Appl Water Sci. 2019 Oct;9(8):171. doi: 10.1007/s13201-019-1053-2
52. Ghasemi M, Naushad M, Ghasemi N, Khosravi-fard Y. Adsorption of Pb(II) from aqueous solution using new adsorbents prepared from agricultural waste: Adsorption isotherm and kinetic studies. J Ind Eng Chem. 2014;20(4):2193-9. doi: 10.1016/j.jiec.2013.09.050
53. Abdel-Ghani NT, Rawash ESA, El-Chaghaby GA. Equilibrium and kinetic study for the adsorption of p-nitrophenol from wastewater using olive cake based activated carbon. Glob J Environ Sci Manag. 2016;2:11-8. doi: 10.7508/gjesm.2016.01.002
54. Langmuir I. The constitution and fundamental properties of solids and liquids. J Franklin Inst. 1917;183(1):102-5. doi: 10.1016/S0016-0032(17)90938-X
55. Krishnamoorthy R, Govindan B, Banat F, Sagadevan V, Purushothaman M, Show PL. Date pits activated carbon for divalent lead ions removal. J Biosci Bioeng. 2019;128(1):88-97. doi: 10.1016/j.jbiosc.2018.12.011
56. Amenaghawon A, Aisien F, Agho O. Adsorption of toluene by waste tyre rubber granules: Effect of operating variables, kinetic and isotherm studies. Int J Sci Res Knowl. 2013;427-38. doi: 10.12983/ijsrk-2013-p427-438
57. Inyinbor AA, Adekola FA, Olatunji GA. Kinetics, isotherms and thermodynamic modeling of liquid phase adsorption of Rhodamine B dye onto *Raphia hookerie* fruit epicarp. Water Resour Ind. 2016;15:14-27. doi: 10.1016/j.wri.2016.06.001

58. Chowdhury S, Misra R, Kushwaha P, Das P. Optimum sorption isotherm by linear and nonlinear methods for safranin onto alkali-treated rice husk. Bioremediat J. 2011 May;15(2):77-89. doi: 10.1080/10889868.2011.570282
59. De La Luz-Asunción M, Sánchez-Mendieta V, Martínez-Hernández AL, Castaño VM, Velasco-Santos C. Adsorption of phenol from aqueous solutions by carbon nanomaterials of one and two dimensions: Kinetic and equilibrium studies. J Nanomater. 2015;2015: 405036. doi: 10.1155/2015/405036
60. Nirmala G, Murugesan T, Rambabu K, Sathiyanarayanan K, Show PL. Adsorptive removal of phenol using banyan root activated carbon. Chem Eng Commun. 2021 Oct;208:831-42. doi: 10.1080/00986445.2019.1674839
61. Shikuku VO, Zanella R, Kowenje CO, Donato FF, Bandeira NMG, Prestes OD. Single and binary adsorption of sulfonamide antibiotics onto iron-modified clay: linear and nonlinear isotherms, kinetics, thermodynamics, and mechanistic studies. Appl Water Sci. 2018;8(6):1-12. doi: 10.1007/s13201-018-0825-4
62. Kannusamy P, Thambidurai S. Synthesis of porous chitosan-polyaniline/ZnO hybrid composite and application for removal of reactive orange 16 dye. Colloids Surfaces B Biointerfaces. 2013;108:229-38. doi: 10.1016/j.colsurfb.2013.03.015
63. Nesic AR, Onjia A, Velickovic SJ, Antonovic DG. Preparation and characterisation of novel biodegradable material based on chitosan and poly (Itaconic Acid) as adsorbent for removal reactive orange 16 dye from wastewater. In: Leal Filho W, Úbelis A, Bērziņa D, editors. Sustainable development, knowledge society and smart future manufacturing technologies. World Sustainability Series. Cham (SZ): Springer; 2015. doi: 10.1007/978-3-319-14883-0_18
64. Jayasantha Kumari H, Krishnamoorthy P, Arumugam TK, Radhakrishnan S, Vasudevan D. An efficient removal of crystal violet dye from waste water by adsorption onto TLAC/Chitosan composite: A novel low cost adsorbent. Int J Biol Macromol. 2017;96:324-33. doi: 10.1016/j.ijbiomac.2016.11.077
65. Feng Y, Dionysiou DD, Wu Y, Zhou H, Xue L, He S, et al. Adsorption of dyestuff from aqueous solutions through oxalic acid-modified swede rape straw: Adsorption process and disposal methodology of depleted bioadsorbents. Bioresour Technol. 2013;138:191-7. doi: 10.1016/j.biortech.2013.03.146
66. Cao JS, Lin JX, Fang F, Zhang MT, Hu ZR. A new absorbent by modifying walnut shell for the removal of anionic dye: Kinetic and thermodynamic studies. 2014 Jul;163:199-205. doi: 10.1016/j.biortech.2014.04.046
67. Fungaro DA, Borrely S, Carvalho TEM. Surfactant modified zeolite from cyclone ash as adsorbent for removal of reactive orange 16 from aqueous solution. Am J Environ Prot. 2013;1(1):1-9. doi: 10.12691/env-1-1-1
68. Jawad AH, Malek NNA, Abdulhameed AS, Razuan R. Synthesis of magnetic Chitosan-Fly Ash/Fe_3O_4 composite for adsorption of reactive orange 16 Dye: Optimization by box–behnken design. J Polym Environ. 2020 Feb;28:1068-82. doi: 10.1007/s10924-020-01669-z
69. Kiran B, Kaushik A. Chromium binding capacity of Lyngbya putealis exopolysaccharides. Biochem Eng J. 2008;38:47-54. doi: 10.1016/j.bej.2007.06.007
70. Febrianto J, Kosasih AN, Sunarso J, Ju YH, Indraswati N, Ismadji S. Equilibrium and kinetic studies in adsorption of heavy metals using biosorbent: A summary of recent studies. J Hazard Mater. 2009;162(2-3):616-45. doi: 10.1016/j.jhazmat.2008.06.042
71. Kim TY, Lee JW, Cho SY. Application of residual brewery yeast for adsorption removal of Reactive Orange 16 from aqueous solution. Adv Powder Technol. 2015;26(1):267-74. doi: 10.1016/j.apt.2014.10.006
72. Rangabhashiyam S, Anu N, Giri Nandagopal MS, Selvaraju N. Relevance of isotherm models in biosorption of pollutants by agricultural byproducts. J Environ Chem Eng. 2014;2(1):398-414. doi: 10.1016/j.jece.2014.01.014
73. Silah H. Adsorption of reactive orange 16 by Amberlyst A21 : Isotherm and kinetic investigations Murat Basar. Turk J Anal Chem. 2020 May;2(1):22-8.
74. Won SW, Choi SB, Yun YS. Performance and mechanism in binding of reactive orange 16 to various types of sludge. Biochem Eng J. 2006;28(2):208-14. doi: 10.1016/j.bej.2005.11.006